Hydromechanical characterization of tide-induced head fluctuations in coastal aquifers: the role of delayed yield and minor permeable layers

Tybaud Goyetche, Maria Pool, Jesus Carrera, Linda Luquot

Title: Hydromechanical characterization of tide-induced head fluctuations in coastal aquifers: the role of delayed yield and minor permeable layers

Tybaud Goyetche[1,2,3], Maria Pool[1,2,4], Jesus Carrera[1,2], Linda Luquot[5]

[1] Institute of Environmental Assessment and Water Research (IDAEA), CSIC, Jordi Girona 18, 08034 Barcelona, Spain

[2] Associated Unit: Hydrogeology group (UPC-CSIC)

[3] Department of Civil and Environment Engineering, Universitat Politècnica de Catalunya (UPC), Jordi Girona 1-3, 08034 Barcelona, Spain

[4] AMPHOS 21 Consulting S. L., 08019 Barcelona

[5] Géosciences Montpellier, Université de Montpellier, CNRS, Place Eugène Bataillon, 34095 Montpellier, France

Abstract

Tidal analysis is an aquifer scale approach that is a low-cost alternative to pumping tests for assessing aquifer hydraulic parameters without groundwater extraction. Many analytical solutions may be used to assess aquifer head fluctuations in response to tidal fluctuations. Nonetheless, they are rarely used in practice. Aside from that, most analytical solutions are based on a conceptual model that typically consists of an unconfined aquifer and a confined aquifer separated by an aquitard, where hydraulic head fluctuations in the unconfined aquifer part are commonly neglected. Additionally, the confined aquifer short response time to sea-level fluctuations cannot rely on the hydraulic connection of the confined aquifer through the aquitard. As a consequence, when

analytical solutions are applied to real-world cases, the hydraulic diffusivity is overestimated. In this study, we investigate through different numerical simulations the fluctuations of the phreatic surface by considering the delayed yield. Numerical results demonstrate that the mechanical effect generated by the load over the bottom of the sea due to sea-level fluctuations is a key factor when determining hydraulic aquifer parameters. We further show that in multilayer systems, head fluctuations in various aquifer layers can cause interferences and, consequently, increased attenuation of the tidal signal, resulting in an overestimation of the inferred hydraulic diffusivity. Our results provide guidance on how to properly reproduce tidal responses in coastal aquifers.

Keywords

Coastal aquifer, water table fluctuations, tidal fluctuations, aquifer characterization, Jacob-Ferris equation, parameter estimation

1. Introduction

As global population soars, economic activities cause significant demand of freshwater resources and coastal aquifers overpumping worldwide, which leads to seawater intrusion (SWI) with major social and economic consequences. Controlling SWI requires detailed characterization of the aquifer and its connection to the sea, which is challenging and costly. Accurate aquifer characterization is essential to design sustainable management schemes and to control or limit the propagation of the seawater wedge (Werner et al., 2013). Traditional hydrogeological tools, such as pumping tests, hydrochemical analyses or geophysical methods, can be used to characterize the coastal

aquifers. However, a singular feature of coastal aquifers is that they respond to sea level fluctuations. These can be wind driven or, usually far more important, caused by astronomical tides. Tides have been studied by humanity for centuries. They are generated by the movement of celestial bodies notably the Moon, around the Earth. causing the rise and fall of sea level.

Tidal response analysis consists of identifying the aquifer geometry and parameters that best explain the observed response to sea-level fluctuations. This response can be viewed as a hydraulic test, which is appealing because of its low-cost (simply set sensors in coastal wells and the sea to monitor fluctuations) and its large-scale (it may allow characterizing the whole coastal zone). Sea level (h_s) fluctuations can be approximated as a sum of harmonics. The response of any linear system to a harmonic stress will also be a harmonic. Therefore, the aquifer response to every harmonic component of tides will be described (Figure 1~~Figure 1~~) by (1) the amplitude damping (A/A_0, ratio of the amplitude observed in the well (A) to the sea level fluctuation amplitude (A_0)); and (2) the time-shift (t_s, delay in time between the fluctuation recorded in the well and the sea level fluctuation). Tidal response analysis consists of deriving hydraulic parameters from the amplitude damping and time-shift from the various tidal harmonics and the available observation points.

The simplest and reference tidal analysis is the one by Jacob (1950) and Ferris (1952) (JF hereinafter), who computed analytically the aquifer response to a harmonic fluctuation of the sea-level by considering a homogeneous, isotropic, and confined aquifer with an infinite inland extent and a vertically connection to the sea at the coastline.

They prescribed head at the coast ($x = 0$) as a harmonic function with a tidal amplitude (A_0, $[L]$) and a tidal period ($\tau = 2\pi/\omega$, $[T]$, where ω $[T^{-1}]$ is the frequency). They found that the response in a well located at a distance x $[L]$ from the coastline is $h(x,t) = A_0 e^{-x/L_c} \sin(\omega t + x/L_c)$, L_c is a characteristic length depending on transmissivity, T $[L^2.T^{-1}]$, and storativity, S [-], such as $L_c = \sqrt{T\tau/\pi S}$. That is, the tidal amplitude decreases exponentially with distance whereas the time-shift increases linearly. Therefore, we can obtain L_c from either the amplitude damping ($ln(A/A_0) = x/L_c$) or the time-shift ($t_s = \omega\, x/L_c$). Knowing L_c, one can obtain $D_h = T/S$ as:

$$D_{h_A} = -\frac{x^2\,\pi}{\tau\left(ln\left(A/A_0\right)\right)^2} \quad (1)$$

$$D_{h_{t_s S}} = \frac{x^2\,\tau}{4\pi\,t_s^2} \quad (2)$$

where D_{h_A} is the hydraulic diffusivity obtained from the amplitude damping and $D_{h_{t_s S}}$ is the one obtained from the time-shift. The two estimates should be identical under the ideal JF assumptions. Note that tidal response analysis does not yield T and S separately but only their ratio, the aquifer hydraulic diffusivity (D_h). Still, D_h is a good indicator of connectivity (Knudby & Carrera, 2006). Furthermore, Slooten et al. (2010) showed that tidal response inland is most sensitive to hydraulic conductivity near the shore. Therefore, by performing this analysis at many observation wells, one can infer which areas are well connected to the sea (i.e., those with high diffusivity), which is relevant because a key issue in coastal aquifer management is where to pump and how much can be pumped.

Tidal response has been coupled with pumping tests to derive spatially varying maps of transmissivity (Alcolea et al., 2007; Alcolea et al., 2009).

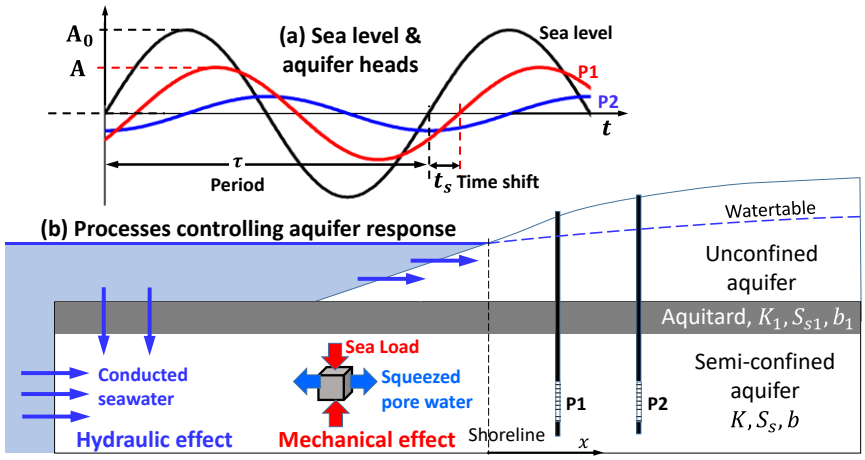

Figure 11 : Factors affecting coastal aquifers level in response to seawater level fluctuations. The aquifer response is damped ($A < A_0$) and shifted (t_s) with respect to sea level. Hydraulic effect (Blue thin arrows) and Mechanical effect (thick arrows)

It is surprising that, given the advantages of the method, its practical application is scarce (Jiao & Tang, 1999; Liu, 1996; Nielsen, 1990; Van Der Kamp, 1972; Zhou et al., 2016). We attribute this paradox to several factors. First and foremost, JF's assumptions may not be appropriate because D_{h_A} and D_{h_S} should be identical whereas, in practice, they are not. This has prompted the derivation of numerous analytical solutions for more complex and realistic aquifer configurations such as confined aquifers connected to the sea far offshore (Guo et al., 2010; Guomin & Chongxi, 1991; Van Der Kamp, 1972), coastal leaky confined aquifers (Chuang & Yeh, 2008; Jeng et al., 2002; Jiao &

a mis en forme : Police :(Par défaut) Times New Roman
a mis en forme : Police :(Par défaut) Times New Roman
a mis en forme : Police :(Par défaut) Times New Roman
a mis en forme : Police :(Par défaut) Times New Roman
a mis en forme : Police :(Par défaut) Times New Roman, Italique
a mis en forme : Police :(Par défaut) Times New Roman

Tang, 1999; Li & Jiao, 2001b, 2002), coastal aquifers with sloping beaches (H. Li et al., 2008; Teo et al., 2003), etc.

Mechanical effects (ME hereinafter) add a further complication to the interpretation of the aquifer response to sea-level fluctuations. A rise in sea level can be viewed as an increase in the load exerted by the sea on the seafloor. According to Terzaghi's (Terzaghi, 1954) theory, this load is initially absorbed by the water as an increase in water pressure. The overpressure is slowly dissipated as water flows away inland (where pressure has not increased) and the load is taken up by the solid skeleton (increase in effective stress), whose porosity is reduced. That is, water is squeezed by the sea load. Acknowledging the mechanical effect has led to a large number of analytical solutions, which require a leaky confined aquifers that extend below the sea and include the effect of the fluctuating load (Geng et al., 2009; G. Li et al., 2008; Li & Jiao, 2001a, 2003a, 2003b; Li et al., 2007). These solutions are integrated and generalized by Guarracino et al. (2012).

The essential feature of these solutions is that (1) the amplitude observed in the aquifer at the coast is about one half of that in the sea (Van Der Kamp, 1972) and (2) the time-shift can be significantly reduced because the squeezing effect of the load is proportional to the time derivative of the sea level, which is largest one quarter of the period before the harmonic maximum (Guarracino et al., 2012; G. Li et al., 2008). Accounting for the mechanical effect is not particularly difficult, but it represents an additional complication. As a result, modelers need to consider under which conditions this effect should be accounted for.

Another feature of equations (1) and (2) is that large damping and time-shift should be observed in unconfined aquifers where D_h is small (large storage coefficient, ~~S~~ [-]). However, significant head responses to tides have been observed several kilometers inland in shallow unconfined coastal aquifers, such as in Spain (Llobregat delta, internal communication, or Argentona aquifer, Martinez et al., 2022), in Hong Kong (Jiao & Li, 2004; Merritt, 2004). We attribute these observations to the slow mobilization of the storage. The storage coefficient of unconfined aquifers consists of two components: an elastic component associated with compression of the aquifer ($S_s b$) and a specific yield (S_y) component associated with pore dewatering. Meinzer (1932) himself pointed "appreciable drainage may occur during a period of several weeks", while discussing of field estimation of S_y (see Dietrich et al. (2018) and Lv et al. (2021)). But the issue was not formalized until it became necessary for the interpretation of pumping wells, when it was labeled "delayed yield" (Boulton, 1954, 1963; Bouwer & Rice, 1978; Neuman, 1972). Delayed yield implies only a fraction of the full storage coefficient (small S) is actually mobilized during a tide period so that the unconfined aquifer reacts as if D_h was larger than in reality. Yet, none of the solutions described above acknowledge delayed yield in tidal response, which we conjecture may be important.

In light of the above considerations, the first relevant question when analyzing the tidal response is how to treat the phreatic surface of the unconfined aquifers. A complementary key question is when the mechanical effect must be considered. The study is aimed at addressing these questions to give guidance on the appropriate conceptual model for the tidal response method. To this end, we performed numerical simulations considering the hydro-mechanical effect generated by tidal fluctuations. Our results aim

at yielding new insights into the tidal method, thus contributing to its application in complex coastal systems.

2. Methods

2.1 Tidal method generalities

2.1.1 Governing equations

Sea level fluctuations cause heads to fluctuate in coastal aquifers hydraulically connected to the sea (Figure 1~~Figure 1~~-A). Aquifer heads also respond to the loading effect of sea level fluctuations on the seafloor. According to Terzaghi's (1954) theory, an increase in loading is initially reflected as an increase in water pressure, and dissipated as water flows away (water is squeezed, Figure 1~~Figure 1~~-B). The mechanical effect can be included in the flow equation as a sink/source term (f) proportional to the time derivative of the total stress (Bear, 1972). For tidal fluctuations, the induced mechanical effect is represented by a sink/source term proportional to the time derivative of seawater level (h_s), expressed as freshwater head (i.e., h_s is the actual sea level fluctuation multiplied by ρ_s/ρ_f, where ρ_s and ρ_f are the densities of seawater and freshwater, respectively). Including this term, fluid mass conservation is given by:

$$S_s \frac{\partial h}{\partial t} = \nabla(K \nabla h) + f \quad (3)$$

$$f = S_s L_e \frac{dh_s}{dt} \quad (4)$$

where S_s is specific storage $[L^{-1}]$; h is aquifer head $[L]$ and the source/sink term f only on the offshore part ($x > 0$, $f = 0$), L_e [-] the tidal loading efficiency. ~~defined by (~~Van der Kamp & Gale~~,~~ (1983) provide a full discussion of this equations and its associated parameters. L_e ~~to~~ describe the formation pressure change caused by a distributed change of pressure at the bottom of the sea (Eq.5), defined by:

$$L_e = \frac{\alpha}{\alpha + \phi\beta} \tag{5}$$

where α is the (oedometric) compressibility of the aquifer skeleton, β is the compressibility of the pore water in the confined aquifer and ϕ porosity [-]. Since coastal sediments are usually young, they are a lot more compressible than water (i.e. $\alpha \gg \beta$). Therefore, we will adopt $L_e = 1$ (see G. Li et al. (2008) and Li et al. (2007) for a collection of values). Note that accounting for this term in numerical models simply requires adding a time varying sink-source term given by Equation (4).

Insight into the nature of this effect can be gained from the analytical solution of Guarracino et al. (2012). They express the tidal response observed in the confined aquifer (h) as the sum of three different components: (i) h_h the direct hydraulic connection where the aquifer opens the sea (horizontal blue arrows at the left of Figure 1~~Figure 1~~), (ii) $h_{h1}$the hydraulic component caused by the indirect connection through the aquitard (vertical blue arrows in Figure 1~~Figure 1~~**),** and (iii) h_m the mechanical component induced by tidal loading (the red arrows in Figure 1~~Figure 1~~ compress the aquifer and squeeze water away, thick blue arrows). Guarracino et al. (2012) analyze them in detail. The three components are shown in Figure 2 for a specific case considering an aquitard with the

following parameters: aquitard thickness (b_1) of 5 m, hydraulic conductivity (K_1) of 0.01 m/d, and a specific storage (S_{s_1}) of $5 \cdot 10^{-4}$ 1/m and a confined aquifer with the following parameters: aquifer thickness (b) of 18 m, hydraulic conductivity (K) of 10 m/d and specific storage (S_s) of $5 \cdot 10^{-5}$ 1/m. Results are shown at the coastline (x = 0 m). Note that, for this example, h_m resembles h whereas the effect of leakage through the aquitard (h_{h1}) is small. However, real-world applications of the Guarracino et al. (2012) analytical solution remain complex and non-trivial. Therefore, to simplify the procedure, in this study we use the principle of superposition over numerical simulations and consider only two hydraulic components of the head response: (1) the hydraulic component (considering h_h and h_{h1} together) and (2) the mechanical contribution. To this end, we adopt a flow model (described in section 1.2) which includes periodic elastic compressions and expansions of the aquitard and the confined aquifer, similar to that of Guarracino et al. (2012) (Figure 3).

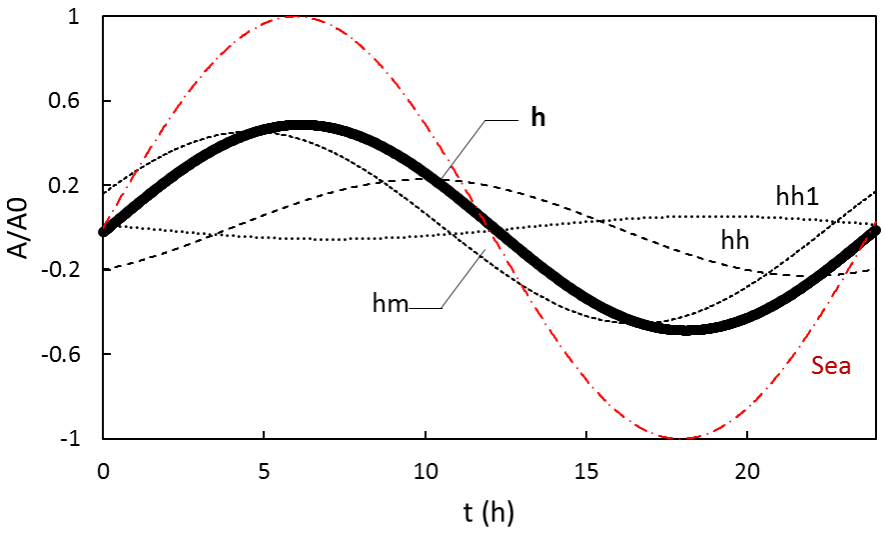

Figure 2 : The aquifer response (h, thick black line) to sea tides (red dashed line) obtain by Guarracino et al. (2012) consists of the superposition of (1) h_h hydraulic connection at the open offshore boundary; (2) h_{h1} hydraulic connection across the aquitard; and (3) h_m hydro-mechanical response. Note that h_m reaches its maximum before sea level.

2.1.2 Phreatic surface and delayed yield

When the specific yield is released instantaneously (i.e., when water content in the unsaturated zone is reduced instantaneously in response to a drop in aquifer head), the phreatic surface boundary condition (Figure 3) is described by:

$$S_y \frac{\partial h}{\partial t}\Big|_{z=h} = -K_z \frac{\partial h}{\partial z} \quad (6)$$

Generally neglected in analytical solutions, the unconfined aquifer phreatic surface also fluctuates with tides even far from the coast just like a confined aquifer. This kind of observation has been largely documented for hydraulic tests (Batu, 1998; Boulton, 1954, 1963; Neuman, 1972). It explains the delayed water table response of unconfined aquifers during a pumping test. Three drawdown phases are observed: (1) Drawdown similar to a confined aquifer (Theis curve with small S) explained by wellbore and the elastic storage, then (2) it reaches a pseudo steady-state (Hantush like) and finally (3) water table decline again (Theis curve with large S). From (3) the specific yield (S_y) can be derived after a long pumping test. In the case of tidal oscillations, phase (1) is observed because it represents instantaneous mobilization of storage, but whether phases (2) and (3) are mobilized depends on the tide period relative to the time it takes to mobilize the

delayed yield. The net result is that the unconfined aquifer acts like a semi-confined. So, if not all the part of the storage is mobilized instantaneously, Eq. 6 becomes Eq. 7.

$$\begin{cases} S_{y0}\dfrac{\partial h}{\partial t} + \displaystyle\sum_{L=1}^{N} S_{y_i}\frac{\partial h_i}{\partial t} = -K_z\frac{\partial h}{\partial z} & \text{(7a)} \\ S_{y_i}\dfrac{dh_i}{dt} = C_i(h - h_i) & \text{(7b)} \end{cases}$$

where S_{y0} is the instantaneous specific yield and the immobile (or slowly yield) zones are characterized by their specific yield (S_{y_i}) and conductance (C_i). Their characteristic time is $1/\alpha_i$ with $\alpha_i = C_i/S_{yi}$. To simplify the analysis, we neglect S_{y0} and consider $N = 1$ so that $S_y = \sum_{i=0}^{N} S_{yi}$ (Boulton, 1963). We solve the system of equation (7) assuming $h = A_0 \sin \omega t$. Then, equation (7b) reads:

$$\frac{dh_f}{dt} = \alpha A_x \sin \omega t - \alpha h_f \tag{8}$$

It is easy to check that the long-term, solution to this equation is:

$$h_f = A_{Sy}\sin(\omega t - \varphi_{Sy}) \tag{9}$$

where $A_{Sy} = A_x(\alpha/\sqrt{\alpha^2 + \omega^2})$, $\varphi_{Sy} = \cos^{-1}(\alpha/\sqrt{\alpha^2 + \omega^2}) = \sin^{-1}(\omega/\sqrt{\alpha^2 + \omega^2})$. This solution points out that h_f behaves, both in terms of damping and time-shift, as if the fraction of specific yield actually mobilized is $\alpha/\sqrt{\alpha^2 + \omega^2}$. If $\alpha \gg \omega$ (i.e. fast response), then, $\varphi_{Sy} \approx 0$, $A_{Sy} = A_x$, and the full specific yield is mobilized (i.e., the aquifer behaves as if it was unconfined). The opposite occurs if $\alpha \ll \omega$, then $A_{Sy} \approx 0$, the aquifer behaves as if it was confined. Finally, if $\alpha \sim \omega$, the aquifer behaves as if it had an intermediate storage coefficient:

$$S_{Dy} = S_0 + S_y \frac{\alpha}{\sqrt{\alpha^2 + \omega^2}} \quad (10)$$

Another, simple approximation to the delayed yield effect can be obtained by observing that, Eq.3 and 4 with BC's (Eq. 7) is a linear system subject to a harmonic fluctuation forcing term. Therefore, any output will also be a harmonic fluctuation with a damped amplitude and a time-shift. To generalize Ferris solution ($h\,(x,t) = A_0 e^{-x/L_c} \sin\,(\omega t + x/L_c)$) we need to acknowledge that both the amplitude and the time-shift will damp, depending on x. We have fitted S to reproduce the additional damping, and found that a solution can be obtained by adopting

$$S_{Dy} = S_s \cdot b + S_y(1 - e^{-\frac{a\tau}{t_{c_z}}}) \quad (11)$$

where b is the aquifer thickness [L], $t_{c_z} = 1/\alpha$, is the vertical characteristic time and a = 0.25, obtained from sensitivity analysis.

2.2 Numerical methodology

In this section, the numerical methodology is presented. Several sets of simulations were carried out to properly define aquifer characterization in coastal aquifers from the tidal method. First, we consider a fully homogeneous confined aquifer similar to the JF conceptual model. Additionally, more complex geometries have been considered in order to (i) simulate properly delayed yield effects and (ii) include layered configurations commonly found in sedimentary systems.

2.2.1 Numerical model setup

An idealized coastal aquifer represented by a 2D vertical section extended 250 m offshore and 750 m onshore is considered in this study. The model domain was discretized into 15.643 triangular elements, refined near the coast and the aquitard portions. We simulate constant density water flow since previous research has shown that density differences have little effect on fluctuations(Ataie-Ashtiani et al.,2001; Slooten et al., 2010). The following boundary conditions were adopted (Figure 3). A Cauchy-type boundary condition was imposed at the inland boundary (considered infinite in the analytical solution). Thus, the inflow/outflow, $Q = \alpha\ (h - H_{ext})\ [L^3.T^{-1}]$, depends on the difference between the calculated head (h, $[L]$) and the reference imposed head at the boundary (H_{ext}, $[L]$, which is taken as zero, since we are only working with fluctuations), and the leakage coefficient (α, $[\mathrm{L}^2/\mathrm{T}]$). This boundary condition reduces the possible impact of boundaries because if the fluctuations reach the inland boundary, then h becomes higher that H_{ext} and water is expelled out of the domain. Two different boundaries (red lines in Figure 3) represent the seaward boundary where the tidal fluctuation of the sea level is assumed to be sinusoidal and simulated with a Dirichlet boundary condition $h_{ss}(t) = A_0 \sin(\omega t)$, with A_0 the amplitude and ω the tidal angular velocity $[T^{-1}]$. In the submerged portion, the mechanical effect was applied through the source and sink terms included as a recharge (f term in Eq.3). Models were run using the TRANSIN code (Medina et al., 2004; Medina & Carrera, 1996) imposing tidal oscillations until the dynamic quasi-steady-state was reached. The boundary conditions in this study differ from those of Guarracino et al. (2012). However, the precision of the

a mis en forme : Police :12 pt

numerical model was tested and verified by comparing the results with conditions equal to those Guarracino et al. (2012) (see details in supplementary materials).

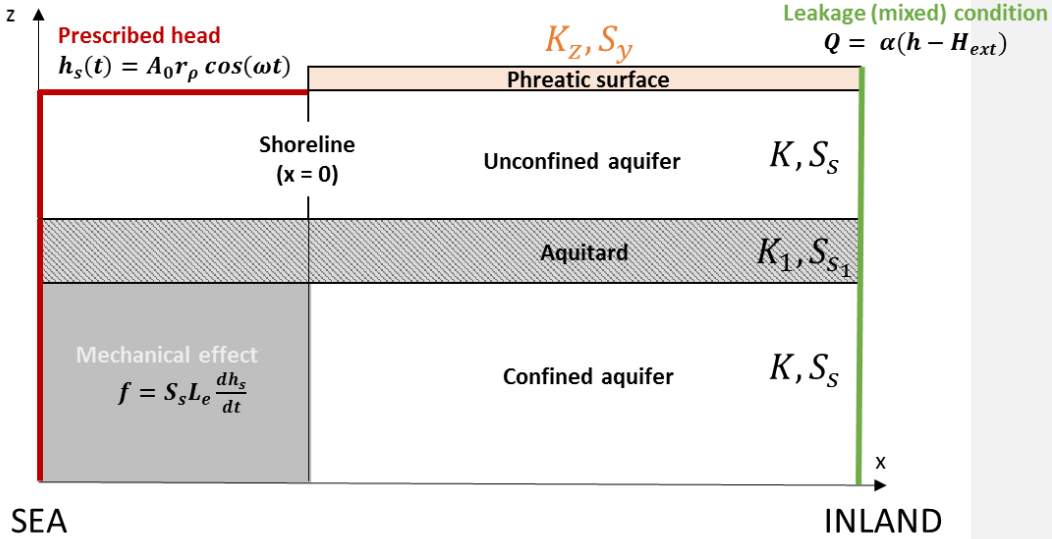

Figure 3: Conceptual model modified from Guarracino et al. (2012) indicating the boundary conditions applied for numerical simulations. Prescribed head is indicated by the red line, the gray rectangle indicates the mechanical boundary condition, the orange rectangle indicates the phreatic surface boundary condition, the inland boundary condition appears in green.

We have simulated several variations of the base case model displayed in Figure 3 to assess the impact of delayed yield and mechanical effect. Table 1~~Table 1~~ summarizes the base case parameters which correspond to a homogeneous confined aquifer (**Erreur ! Source du renvoi introuvable.**~~Figure 4~~a). We varied the geometry and parameters to analyze the impact of the mechanical effect and the delayed yield. We simulated three sets of configurations: single aquifer (i.e., no aquitard), double aquifer (one aquitard) and

a mis en forme : Police :Non Gras

Code de champ modifié

multi-aquifer (several aquitards) systems. For each of these three systems, we considered three configurations. They are summarized in **Erreur ! Source du renvoi introuvable.**~~Figure 4~~ and explained in the following. In all simulations, aquifers and aquitards hydraulic parameters (K_x and S_s) are conserved. Moreover, they are both considered isotropic, so that $K_x = K_z$.

Table 1: Parameters used in the base case simulation

Parameter	Value	Description
L_x (m)	1000	Domain x length
L_z (m)	35	Domain z thickness
A_0 (m)	1	Tidal amplitude
τ (h)	23.9	Tidal period
K (m/d)	10	Aquifer permeability or hydraulic conductivity
S_s (1/m)	5e-5	Aquifer specific storage
K_1 (m/d)	0.01	Aquitard permeability
S_{s1} (1/m)	5e-4	Aquitard specific storage
H_{ext} (m)	0	Reference external head
α (m^2/d)	0.1	Leakage coefficient inland
D (m)	250	Offshore aquifer extension

Code de champ modifié

a mis en forme : Police :Non Gras

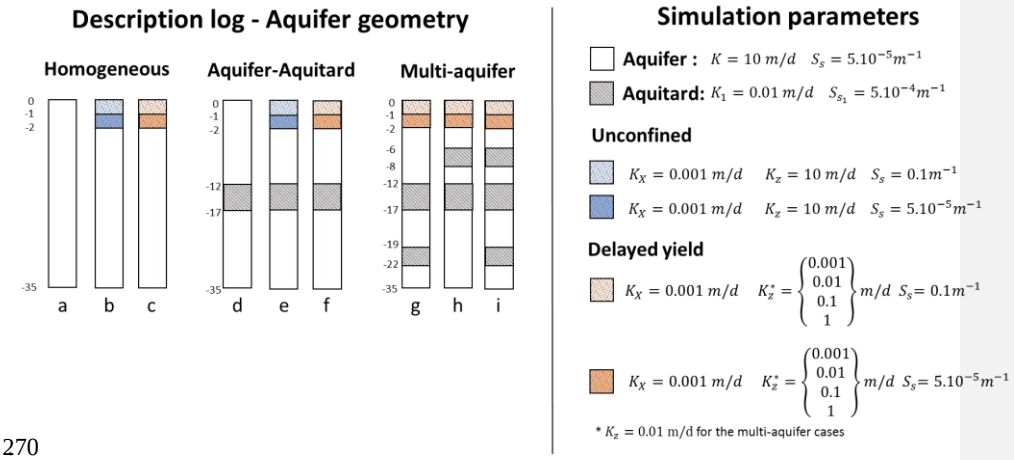

Figure 4: Simulation cases (presented in the form of geological logs in the inland portion) and parameters; Homogeneous cases: (a) confined (Base case), (b) unconfined, and (c) delayed yield; Two Aquifers cases: (d) confined, (e) unconfined, and (f) delayed yield; and Multi-aquifer systems: (g) 2 aquitards with a thick unconfined aquifer, (h) 2 aquitards with a thin unconfined aquifer, and (i) 3 aquitards. Single aquifer: the effect of delayed yield

2.2.2 Single aquifer: the effect of delayed yield

To assess the effect of delayed yield , we analyze three configurations varying the treatment of the phreatic surface : (a) fully confined (i.e., no specific yield, **Erreur ! Source du renvoi introuvable.**~~Figure 4~~a) (Base case), (b) free surface (i.e., instantaneous yield, **Erreur ! Source du renvoi introuvable.**~~Figure 4~~b) and (c) delayed yield (**Erreur ! Source du renvoi introuvable.**~~Figure 4~~c). The confined aquifer (a) is simulated by setting a no-flow boundary condition at the top of the aquifer. For cases b and c we adopt the approach of Carrera and Neuman (1986), which requires a geometry modification in the inland part of the model including two thin layers at the top with a thickness of 1 m

each. In the additional layers the permeability is assumed to be anisotropic ($K_x << K_z$), such that the main component of the flow is vertical. If the hydraulic conductivity of these layers is high, the aquifer behaves as unconfined. Otherwise, yield is delayed with a characteristic time, $t_{cz} = S_y L_z / K_z$, where L_z = 2 m.

Hydraulic parameters applied to the unconfined (b) and delayed yield (c) cases are presented in **Erreur ! Source du renvoi introuvable.**~~Figure 4~~. A unique K_x value is considered for these additional layers. We considered four values for the vertical permeability (K_z) to study the sensitivity of the delayed yield boundary condition directly affecting its characteristic time (t_{c_z}). The resulting values of t_{c_z} are: 0.1, 1, 10, and 100 days.

2.2.3 Double aquifer system: mechanical and delayed yield effects

Three configuration of a double aquifer system are considered by including an aquitard (b_1= 5 m) between an upper unconfined aquifer and a lower confined (actually semi-confined) aquifer, while varying the simulation of phreatic surface of the upper aquifer (**Erreur ! Source du renvoi introuvable.**~~Figures 4~~-d to f). This conceptual model is similar to the one presented by Guarracino et al. (2012). This aquifer configuration is considered to (1) assess the impact of the upper aquifer delayed yield on the deep aquifer, and (2) examine the effectiveness of the mechanical component. Furthermore, the simulation with the phreatic surface as delayed yield (**Erreur ! Source du renvoi introuvable.**~~Figure 4~~-f) was duplicated with and without the mechanical effect by removing the recharge term applied offshore.

2.2.4 Multi-Aquifer system

Finally, more realistic simulations are considered with three or more aquifer units separated by semi-permeable layers (**Erreur ! Source du renvoi introuvable.**~~Figure 4~~ g to i). Multilayered aquifers are commonly observed in coastal aquifers due to sequential sedimentation. For these simulations, a vertical permeability of K_z = 0.01 m/d is adopted for the delayed yield boundary, so that the equivalent t_{c_z} is 10 days.

3. Results and discussion

We simulate all the configurations described above by assuming that sea level fluctuates as a sinusoidal wave with a period of 23.9 days. Given the linearity of the system, results are always a sinusoidal head damped and lagged with respect to the sea, as shown in Figure 1. Therefore, rather than showing the head evolution, we will simply discuss amplitude damping and time-shift. In general, tidal fluctuations will contain several harmonics (i.e., sea level will be equal to the sum of several harmonics, each with its own period), but each will similarly to the one we discuss here.

3.1 Single aquifer: the role of delayed yield

Figure 5 displays the hydraulic diffusivity one would obtain when using amplitude damping (D_{h_A}, Eq. 1) or time-shift ($D_{h_{tS_S}}$, Eq. 2). As a reference, we also display the true hydraulic diffusivity ($D_h = T/S$), that is the one calculated using the parameters indicated in **Erreur ! Source du renvoi introuvable.**~~Figure 4~~. For the delayed yield case, not all storage is mobilized during a tidal cycle, therefore diffusivity is computed using the "apparent" specific yield given by Eq. 10.

The fact that the observation points are located at some depth implies that there will be some amplitude damping and time-shift, even close to the shore. Therefore, Equations 1 and 2 would yield zero diffusivity for $x = 0$. To illustrate this point, we show in Figure 6 the velocities computed at the tidal maximum for a confined, an unconfined and a delayed yield. Velocities only become horizontal (i.e., according to Dupuit's approximation) in the confined case. In order to address this vertical component of water flux, we substitute x in equations 1 and 2 by $x_{corr} = \sqrt{x^2 + z^2}$. Note that this correction helps somewhat near the shore, but become irrelevant when x is much larger than z .

The estimated hydraulic diffusivities for the confined case are similar to the "true" ones (see D_h conf. in Figure 5, represented by dotted blue line), only a bit smaller because of the vertical component of flux near the shore shown in Figure 6, confined case. This translates into a small damping in amplitude and shift in time at the deep observation well. The additional energy dissipation caused by the vertical water flux causes the estimated D_h to be slightly smaller than the "true" one. These results confirm those of Todd (1980) and Erskine (1991).

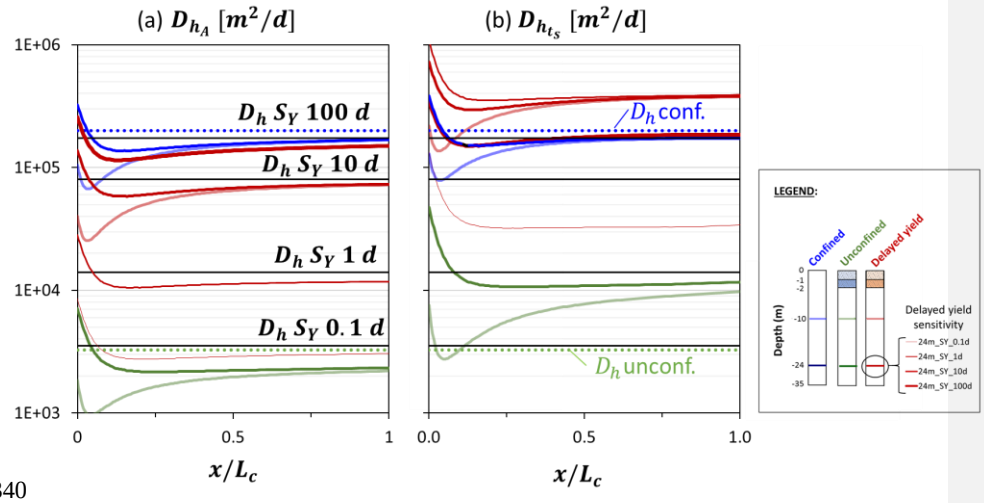

Figure 5: Hydraulic diffusivity estimated from (a) amplitude damping (D_{h_A}) and (b) the time-shift ($D_{h_{t_s}}$) for the single aquifer case with a confined (blue lines), unconfined (green lines) or a delayed yield (red lines) phreatic surface. Results are presented versus dimensionless distance from the coast (x/L_c, where L_c is the characteristic distance of every case). As a reference, true hydraulic diffusivities are shown for (a) confined aquifer (D_h conf., blue dotted line), (b) unconfined aquifer (D_h unconf., green dotted line), and (c) delayed yield cases (black lines, identified by the characteristic delayed yield time). Light colors represent observations at z = -10 m and dark colors at z = -24 m. Sensitivity of the delayed yield is presented in dark red lines with an increasing line thickness with the t_{c_z} tested values (0.1, 1, 10 and 100 days).

The two other cases (unconfined and delayed yield) are more shifted with respect to D_h conf. in Figure 5.

The effect of delayed yield is non-trivial. A long characteristic time implies that only a small fraction of storativity is mobilized. As expected, amplitude damping is only

a bit larger than the confined case (Figure 5a, $t_{c_z} = 100\ days$), and hydraulic diffusivity obtained from the amplitude damping is a bit smaller than the confined case. This explains why a tidal response has been observed far inland in unconfined aquifers (Jha et al. 2008; Solórzano-Rivas et al., 2021; Vallejos et al., 2015). However, the result is opposite in terms of time-shift (t_s), delayed yield seems to accelerate the signal propagation. While one would expect, a lower amplitude to cause a higher t_s including the delayed yield leads to smaller time-shift compared to the confined case leading to D_h values higher than D_h conf. (Figure 5-b). This result highlights that diffusivities resulting from the time-shift are less accurate than those obtained from the amplitude damping.

Increasing the delayed yield vertical characteristic time (t_{c_z}), leads to values of D_{h_A} and $D_{h_{t_s}}$ that are close to D_h conf.. Similarly, when a small t_{c_z} is applied, the phreatic surface presents an unconfined behavior. In all cases, the approximation of ~~E~~equation (10) works reasonably well for the mobilized specific yield.

Most analytical solutions neglect changes in the vertical dimension. However, the analysis of head responses at two different depths (z= -10 m and -24 m) shows some vertical differences in the 3 cases. Thus, strong vertical differences in the unconfined case are observed, even at distance from the coast (Figure 5). These differences are more significant for the time-shift (Figure 5b).This effect has been described for aquifers placed below a confining layer that is connected to a free surface, designated as “capillary exposed surfaces” (Bear, 1972).

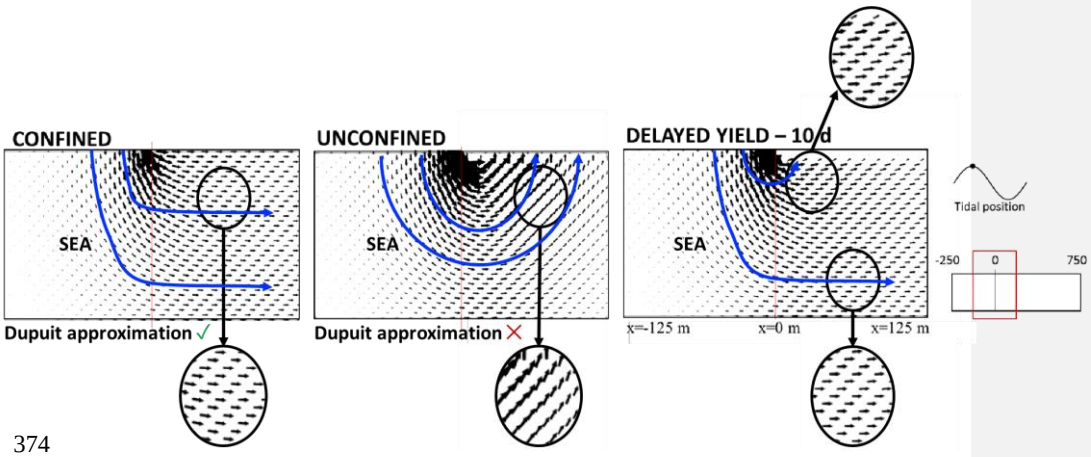

374

375 Figure 6: Velocity fields for the homogeneous simulations. To emphasize vertical features, too

376 small to identify relative to the horizontal scale, the vertical component is exaggerated by a

377 factor of 2.

378

3.2 Double aquifer system. Mechanical effect

Hydraulic diffusivity results for the case in which the aquifer is split by one aquitard layer are presented in Figure 7. These results are complemented with maps of the velocity fields (Figure 8), and a map of the amplitude damping factor (A/A_0) and the dimensionless time-shift (ωt_s) (Figure 9).

Hydraulic diffusivities of the upper aquifer derived from 10 m deep (light color in Figure 7 for z = -10 m) are smaller than for the single aquifer case, in both estimations (from damping and time-shift). That is, the presence of the deep aquifer leads to additional damping and time-shift. Note that the true D_h for the confined case (D_h conf. in Figure 7) remains unchanged, but a D_h is underestimated by a factor of 4 for the confined case and 2.5 for the delayed yield case (note that D_h Sy 10 d is reduced because transmissivity is proportional to thickness, whereas the mobilized specific yield does not depend on thickness). The unconfined case (light green line in Figure 7) is more interesting. D_h is slightly underestimated for short distances, but becomes over estimated for distances larger than 0.4 L_c (recall that L_c in Figure 7 is the one corresponding to the confined aquifer, or some 250m, so that $0.4L_c \approx 3L_{c\_unc}$). That is, the distance where D_{h_A} (and also $D_{h_{t_s}}$) starts increasing coincides with the distance where the response along the upper aquifer becomes negligible. This suggests that the response observed is the one transferred from the deep aquifer (i.e., interference). Moreover, the break observed in the curve as well as the precision of D_h after this distance cannot be considered since the fluctuations are almost completely attenuated (0.02% of A_0). Numerically it would require a mesh refinement for better accuracy.

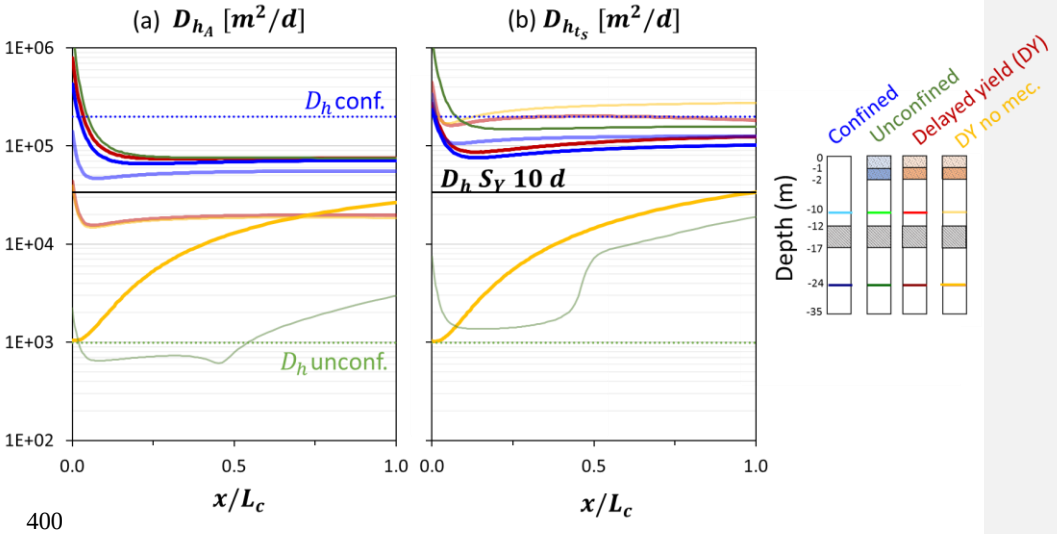

Figure 7: Hydraulic diffusivity estimated from (a) amplitude damping (D_{h_A}) and (b) the time-shift ($D_{h_{t_s}}$) for a two aquifers system. Differences results from the phreatic surface: confined (blue lines), unconfined (green lines), and a delayed yield (red lines) phreatic surface. Also, a delayed yield phreatic surface with no mechanical effect is presented (yellow lines). (a) Hydraulic diffusivity estimated from amplitude damping (D_{h_A}). (b) Hydraulic diffusivity estimated from the time-shift ($D_{h_{t_s}}$). They are presented versus dimensionless distance from the coast (x/L_c). Dotted lines represent the hydraulic diffusivity for a confined aquifer (blue) and for an unconfined aquifer (green). The black line represents the hydraulic diffusivity for the delayed yield for a vertical characteristic time of 10 d. Light colors represent observation at z = -10 m and dark colors at z = -24 m (mostly collapsed at the top of figure near D_h conf.).

The mechanical effect is apparent in the maps of velocities, A/A_0 and ωt_s (Figure 8 and Figure 9). Mechanically driven flux in the deep aquifer is relevant from an offshore distance of the order of L_c. When the mechanical effect is neglected, flux is only relevant

414 near the offshore portion of the deep aquifer. Therefore, we must conclude that the
415 observed flux is mechanically driven. The impact of this flux in terms of time-shift is
416 moderate, but it is large in terms of amplitude. For the parameters of this example, there
417 is a positive time-shift at the shore (maximum response slightly delayed with respect to
418 the sea level maximum). Recall that the shift was negative for the parameters of Figure
419 2. Also, A/A_0 is slightly smaller than 0.5 at the shore. Still, for the computation is
420 diffusivities in all deep observation wells we have divided the sea level amplitude by a
421 factor of 2 to acknowledge the mechanical effect. The results appear to be adequate in
422 that the order of magnitude of the computed diffusivities is correct. The velocities display
423 several interesting features. First, they display a slight vertical downwards component in
424 the offshore portion, just below aquitard, despite the fact that no flux is apparent in the
425 upper aquifer. They also display a slight upwards component deep inland. In fact, though
426 hardly visible, flow in the aquitard is vertical and away from the center, which shows the
427 squeezing effect. Second, flux in the offshore portion of the aquifer is negligible when
428 the mechanical effect is acknowledged, but downwards when it is not. This suggests that
429 the hydraulic conductance effect caused by head fluctuations at the boundary is balanced
430 by the squeezing effect (loading causes all heads to fluctuate simultaneously). The
431 aquitard hinders vertical conductance of water across, so that the dominant flux below is
432 essentially mechanical. An implication of this finding is that the mechanical effect should
433 always be included in models (nothing is lost when it is irrelevant).

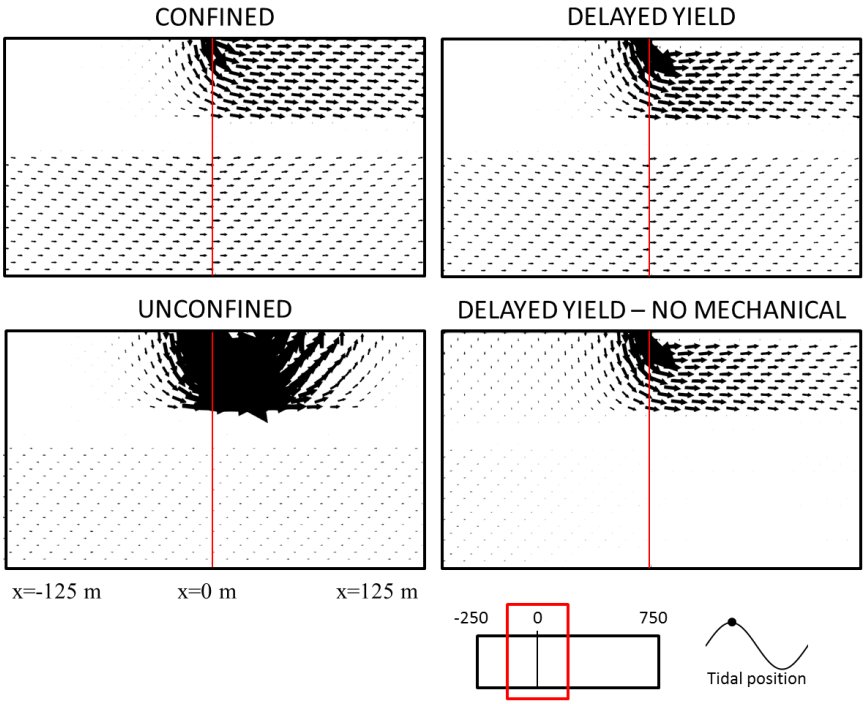

Figure 8: Velocity fields for the two aquifers simulations. The delayed yield case has also been simulated without mechanical effect. To emphasize vertical features, too small to identify relative to the horizontal scale, the vertical component is exaggerated by a factor of 2.

In spite of the above complexities, estimates of D_h are not quite good. D_{h_A} is some 3 times smaller than the confined aquifer D_h, virtually identical for the three cases (conf., unconf., and delayed yield). This similarity despite the above mentioned aquifer interference, suggests that interference has a moderate effect there the signal is strong. D_{h_s} is closer than D_{h_A} to the time value, but the estimates are more sensitive to the upper aquifer conditions. This implies that interference is more important for time-shift than for amplitude damping.

Two additional comments must be made. First, ignoring the mechanical effect does not affect D_{h_A} estimates in the upper aquifer, but they do affect somewhat estimates of $D_{h_{t_s}}$. Neglecting the mechanical effect in the deep aquifer is not acceptable.

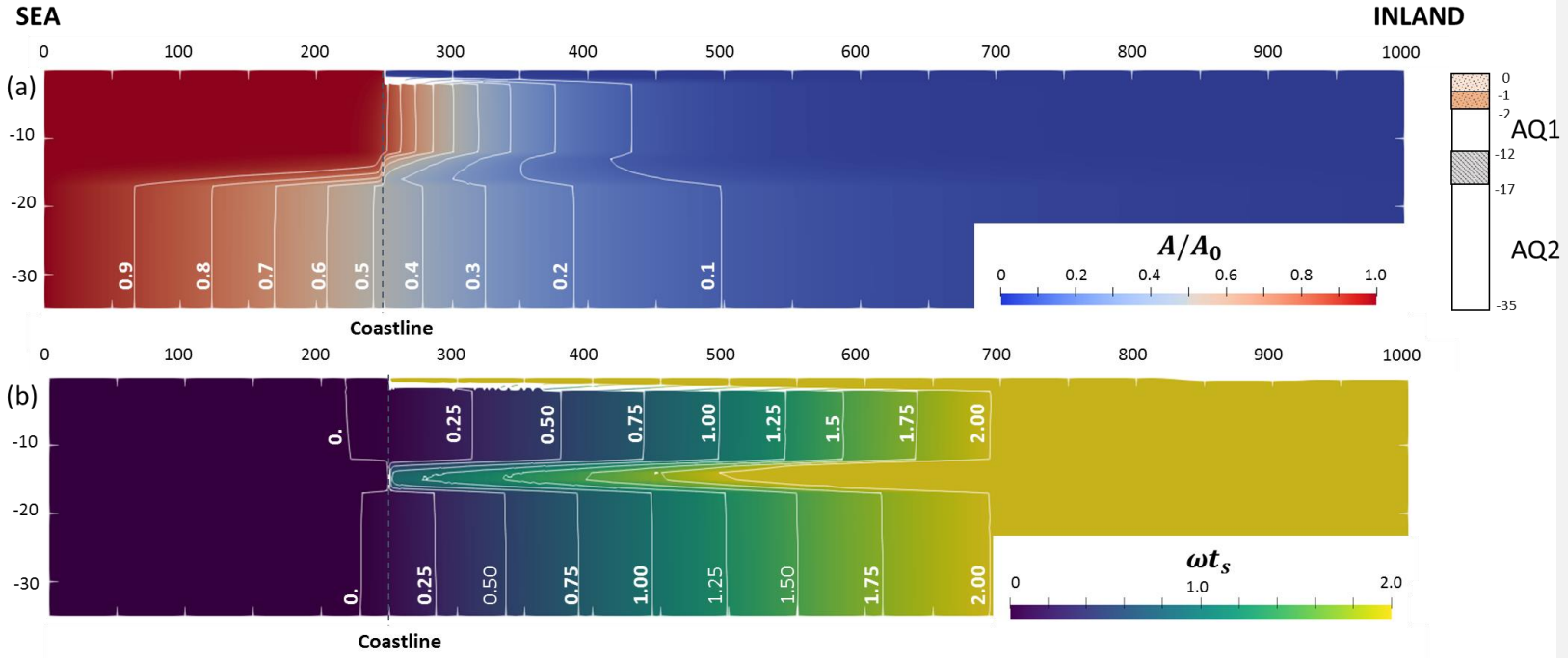

Figure 9: Amplitude attenuation (a) and dimensionless time-shift (b) distribution over the domain simulated for an aquifers-aquitard system with delayed yield

3.3 Multilayered aquifer

Results for the multilayer cases are presented in Figure 10 and complemented with velocity fields in Figure 11. Results for the shallow aquifers, here represented by : (i) two cases with a 10 m thick aquifer (cases a and b), and (ii) two cases with 1 m thick aquitard dividing these upper aquifer (cases b and d). When we observe at 5 m depth, all the simulations present an underestimation of D_{h_A} with respect to the true D_h. which reflects that water flux into/out of aquitards is more significant. From the time-shift, $D_{h_{t_s}}$ is overestimated up to 1 order of magnitude. Moreover, we observed differences at high distance between cases with the same shallow aquifer geometry. The only difference in these cases is their deep aquifer geometry, indicating the influence of deeper layers. Observations at 10 m depth presents some D_{h_A} values similar to results of deeper aquifers. This is not the case, in terms of time-shift.

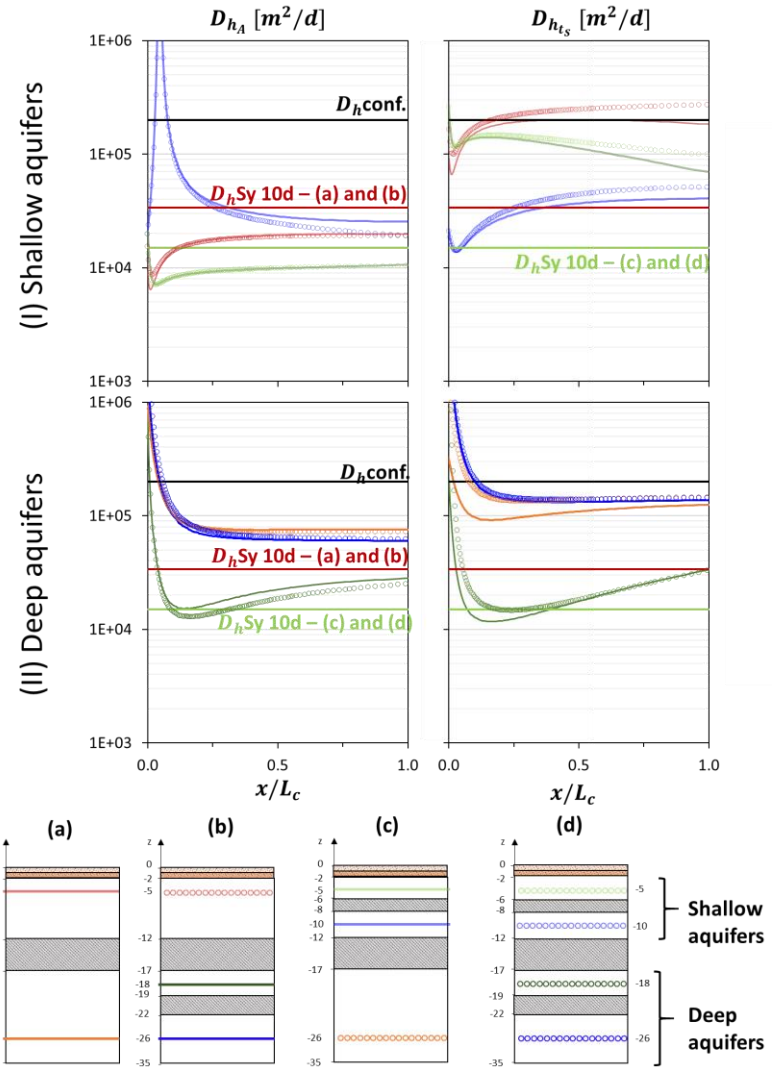

461 .

462 Figure 10: Estimated hydraulic diffusivity for multilayered aquifers with 4 different cases (a, b, c,
463 and d). (I) Hydraulic diffusivity estimated at 5 and 10 m. (II) Hydraulic diffusivity estimated at 18
464 and 26 m depth. They are presented versus dimensionless distance from the coast (x/L_c). We
465 indicate aquifers with similar geometry by a same color with one case with a full line and one

case with round unfilled markers. Thus, at -10 m cases a and b are presented in light red and c and d in light green; at -10 m cases c and d are presented in light blue; then at -18 m cases b and d are in dark green and finally at -26 m cases a and c are presented in orange and b and d in dark blue.

In deep aquifers, the considered cases are representing a large confined aquifer (cases a and c) with 18 m of aquifer thickness and a system with a 3 m aquitard diving two aquifers (cases b and d). We observed in deeper layers similar results as previously with value tending to D_h conf. for observation at 26 m depth. These results are reflected in the velocity fields, similar for all cases in the deeper aquifer (Figure 11). Therefore, the observation at 18 m (cases b and d) are largely underestimating this value. Indicating that fluctuations are rapidly damped, confirmed by their velocity fields. An interesting feature of the velocity fields is that water fluxes are much larger in the thin than in the thick aquifers. This reflects the much higher specific storage of the aquitards, which implies a significant squeezing flux. This flux is reduced when distributed over a thick aquifer but can be large in thin aquifers (larger than that in the upper aquifer where it results from direct hydraulic connection to the sea).

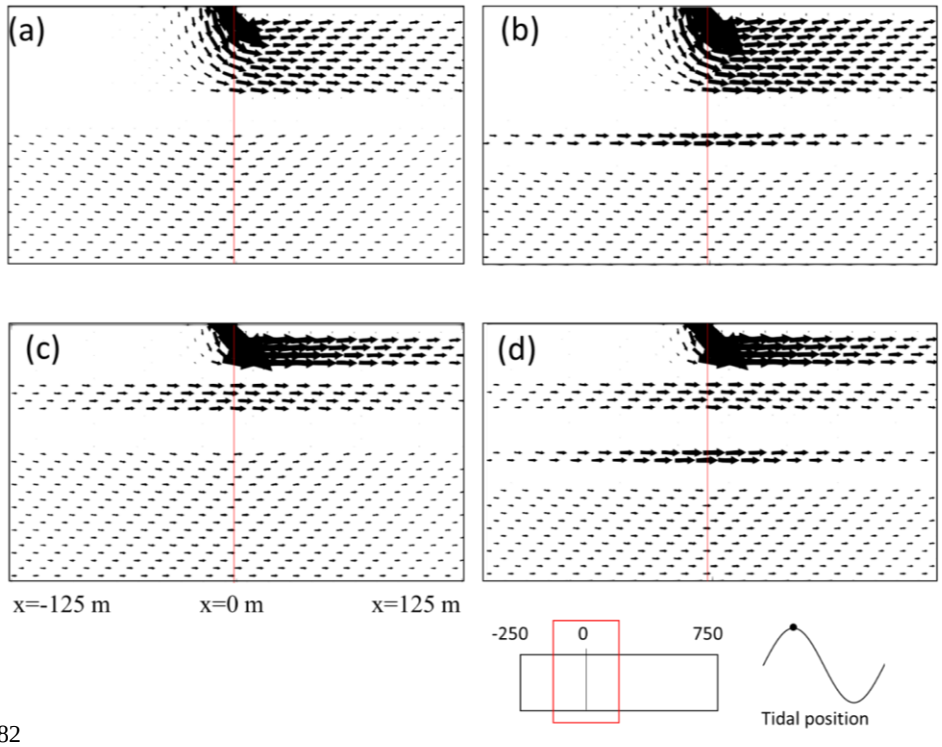

482

483 Figure 11: Velocity fields for the multilayered aquifers. To emphasize vertical features, too small

484 to identify relative to the horizontal scale, the vertical component is exaggerated by a factor of

485 2. Letters refers to cases presented in Figure 10.

4. Conclusion

Recent research on tidal methods to characterize the hydrodynamic parameters and connectivity to the sea in coastal aquifers has provided a more complete understanding of the aquifer response to tidal fluctuations. Current findings suggest that various components must be considered, such as the hydraulic part of the response combined with the mechanical effect due to loading and unloading on the submerged portion of the aquifer system. However, various open questions remained regarding the consideration of some part of the system (unconfined aquifer) or due to the vague and weak provisions about the mechanical effect. More importantly, delayed yield has been ignored in tidal response research. These questions hinder applicability of tidal response methods to real cases.

In this study, we have systematically analyzed the impact of the mechanical effect and delayed yield on the response to tidal fluctuations in coastal aquifers. To this end, different aquifer configurations and boundary conditions have been considered. Our results demonstrate that the order of magnitude of hydraulic diffusivity is well reproduced when using the JF equation based on amplitude damping provided that two precautions are adopted: (1) near the shore, the actual distance to the shore (including the vertical component) should be adopted, (2) in deep aquifers, where the response is mechanically controlled, the sea level amplitude should be divided by two. The time-shift is affected by numerous factors (interference, depth, phreatic surface) and we have not found a way to account for them in an easy manner. But even if an appropriate D_h can be found, the problem lies on its interpretation. If the aquifer is unconfined and the modeler assume

$T = D_h S$, with $S = S_s b + S_y$, then actual transmissivity can be overestimated by orders of magnitude, because the effectively mobilized storativity can be far smaller than the specific yield, which should be expected always. This point highlights the need to perform relatively long pumping tests to complement tidal response analysis for robust identification of coastal aquifer parameters.

The mechanical effect must be acknowledged below aquitards. Deep aquifers react rapidly to tides, even faster than the shallow aquifer. The mechanical effect is relevant even in relatively thin aquitards. Moreover, numerical results reveal the presence of interferences between layers in multi-layered systems. The result is that the behavior can be too complex for analytical solutions and implies the need for numerical modeling. In fact, the conclusion that tidal response interpretation is complicated by numerous factors implies that it contains information about all of them, so that it is worth including tidal response data in any modeling effort. While this may sound too complex, modeling the mechanical effect only implies adding a relatively easy sink-source term. Its simplicity leads us to recommend always including it, as nothing is lost when the mechanical effect is irrelevant.

This study focused only on simple sinusoidal sea-level fluctuations in coastal aquifers. Further analysis considering real aquifer geometries and real sea-level fluctuations with multiple harmonics should be examined in future investigations.

Acknowledgement

We acknowledge the Spanish Ministry of Economy, Industry and Competitiveness to fund this work through projects CGL2013-48869-C2-1-R/2-R and CGL2016-77122-C2-1-R/2-R and for the PhD fellowship (BES-2017-080028) from the FPI Program awarded to T. Goyetche. We also thank two reviewers for their valuable comments.

Bibliography

Alcolea, A., Castro, E., Barbieri, M., Carrera, J., & Bea, S. (2007). Inverse modeling of coastal aquifers using tidal response and hydraulic tests. *Groundwater*, *45*(6), 711-722.

Alcolea, A., Renard, P., Mariethoz, G., & Bertone, F. (2009). Reducing the impact of a desalination plant using stochastic modeling and optimization techniques. *Journal of Hydrology*, *365*(3-4), 275-288.

Ataie-Ashtiani, B., Volker, R., & Lockington, D. (2001). Tidal effects on groundwater dynamics in unconfined aquifers. *Hydrological Processes*, *15*(4), 655-669.

Batu, V. (1998). *Aquifer hydraulics: a comprehensive guide to hydrogeologic data analysis*: John Wiley & Sons.

Bear, J. (1972). *Dynamics of fluids in porous media*: Dover Publications.

Boulton, N. S. (1954). The drawdown of the water-table under non-steady conditions near a pumped well in an unconfined formation. *Proceedings of the Institution of Civil Engineers*, *3*(4), 564-579.

545 Boulton, N. S. (1963). Analysis of data from non-equilibrium pumping tests allowing for
546 delayed yield from storage. *Proceedings of the Institution of Civil Engineers*,
547 *26*(3), 469-482.
548 Bouwer, H., & Rice, R. C. (1978). Delayed aquifer yield as a phenomenon of delayed air
549 entry. *Water Resources Research*, *14*(6), 1068-1074.
550 Carrera, J., & Neuman, S. P. (1986). Estimation of aquifer parameters under transient and
551 steady state conditions: 3. Application to synthetic and field data. *Water*
552 *Resources Research*, *22*(2), 228-242.
553 Chuang, M.-H., & Yeh, H.-D. (2008). Analytical solution for tidal propagation in a leaky
554 aquifer extending finite distance under the sea. *Journal of Hydraulic Engineering*,
555 *134*(4), 447-454.
556 Dietrich, S., Carrera, J., Weinzettel, P., & Sierra, L. (2018). Estimation of specific yield
557 and its variability by electrical resistivity tomography. *Water Resources Research*,
558 *54*(11), 8653-8673.
559 Erskine, A. D. (1991). The effect of tidal fluctuation on a coastal aquifer in the UK.
560 *Groundwater*, *29*(4), 556-562.
561 Ferris, J. G. (1952). *Cyclic fluctuations of water level as a basis for determining aquifer*
562 *transmissibility*. Retrieved from Washington, D.C.:
563 Geng, X., Li, H., Boufadel, M. C., & Liu, S. (2009). Tide-induced head fluctuations in a
564 coastal aquifer: effects of the elastic storage and leakage of the submarine outlet-
565 capping. *Hydrogeology Journal*, *17*(5), 1289-1296.
566 Guarracino, L., Carrera, J., & Vázquez-Suñé, E. (2012). Analytical study of hydraulic and
567 mechanical effects on tide-induced head fluctuation in a coastal aquifer system

that extends under the sea. *Journal of Hydrology, 450-451*, 150-158. doi:10.1016/j.jhydrol.2012.05.015

Guo, H., Jiao, J. J., & Li, H. (2010). Groundwater response to tidal fluctuation in a two-zone aquifer. *Journal of Hydrology, 381*(3-4), 364-371. doi:10.1016/j.jhydrol.2009.12.009

Guomin, L., & Chongxi, C. (1991). Determining the length of confined aquifer roof extending under the sea by the tidal method. *Journal of Hydrology, 123*(1-2), 97-104.

Jacob, C. E. (1950). Engineering hydraulics. *Flow of ground waterJohn Wiley and Sons, New York*, 321-386.

Jeng, D.-S., Li, L., & Barry, D. A. (2002). Analytical solution for tidal propagation in a coupled semi-confined/phreatic coastal aquifer. *Advances in Water Resources, 25*(5), 577-584.

Jha, M. K., Namgial, D., Kamii, Y., & Peiffer, S. (2008). Hydraulic parameters of coastal aquifer systems by direct methods and an extended tide–aquifer interaction technique. *Water resources management*, 22(12), 1899-1923.

Jiao, J. J., & Li, H. (2004). Breathing of coastal vadose zone induced by sea level fluctuations. *Geophysical Research Letters, 31*(11).

Jiao, J. J., & Tang, Z. (1999). An analytical solution of groundwater response to tidal fluctuation in a leaky confined aquifer. *Water Resources Research, 35*(3), 747-751.

589 Knudby, C., & Carrera, J. (2006). On the use of apparent hydraulic diffusivity as an
590 indicator of connectivity. *Journal of Hydrology*, *329*(3), 377-389.
591 doi:https://doi.org/10.1016/j.jhydrol.2006.02.026
592 Li, G., Li, H., & Boufadel, M. C. (2008). The enhancing effect of the elastic storage of
593 the seabed aquitard on the tide-induced groundwater head fluctuation in confined
594 submarine aquifer systems. *Journal of Hydrology*, *350*(1-2), 83-92.
595 doi:10.1016/j.jhydrol.2007.11.037
596 Li, H., Boufadel, M. C., & Weaver, J. W. (2008). Tide-induced seawater–groundwater
597 circulation in shallow beach aquifers. *Journal of Hydrology*, *352*(1-2), 211-224.
598 Li, H., & Jiao, J. J. (2001a). Tide-induced groundwater fluctuation in a coastal leaky
599 confined aquifer system extending under the sea. *Water Resources Research*,
600 *37*(5), 1165-1171. doi:10.1029/2000WR900296
601 Li, H., & Jiao, J. J. (2001b). Analytical studies of groundwater-head fluctuation in a
602 coastal confined aquifer overlain by a semi-permeable layer with storage.
603 *Advances in Water Resources*, *24*(5), 565-573.
604 Li, H., & Jiao, J. J. (2002). Analytical solutions of tidal groundwater flow in coastal two-
605 aquifer system. *Advances in Water Resources*, *25*(4), 417-426.
606 doi:10.1016/S0309-1708(02)00004-0
607 Li, H., & Jiao, J. J. (2003a). Influence of the tide on the mean watertable in an unconfined,
608 anisotropic, inhomogeneous coastal aquifer. *Advances in Water Resources*, *26*(1),
609 9-16. doi:10.1016/S0309-1708(02)00097-0

Li, H., & Jiao, J. J. (2003b). Tide-induced seawater–groundwater circulation in a multi-layered coastal leaky aquifer system. *Journal of Hydrology*, *274*(1-4), 211-224. doi:10.1016/S002-1694(02)00413-4

Li, H., Li, G., Cheng, J., & Boufadel, M. C. (2007). Tide-induced head fluctuations in a confined aquifer with sediment covering its outlet at the sea floor. *Water Resources Research*, *43*(3).

Liu, K.-F. (1996). Tide-induced ground-water flow in deep confined aquifer. *Journal of Hydraulic Engineering*, *122*(2), 104-110.

Lv, M., Xu, Z., Yang, Z. L., Lu, H., & Lv, M. (2021). A comprehensive review of specific yield in land surface and groundwater studies. *Journal of Advances in Modeling Earth Systems*, *13*(2), e2020MS002270.

Martínez-Pérez, L., Luquot, L., Carrera, J., Marazuela, M. A., Goyetche, T., Pool, M., Palacios, A., Bellmunt, F., Ledo, J., Ferrer, N., del Val, L., Pezard, P. A., García-Orelllana, J., Diego-Feliu, M., Rodellas, V., Saaltink, M.W., Vázquez-Suñé, E., & Folch, A. (2022). A multidisciplinary approach to characterizing coastal alluvial aquifers to improve understanding of seawater intrusion and submarine groundwater discharge. *Journal of Hydrology*, 127510.

Medina, A., & Carrera, J. (1996). Coupled estimation of flow and solute transport parameters. *Water Resources Research*, *32*(10), 3063-3076.

Medina, A., & Carrera, J. (2003). Geostatistical inversion of coupled problems: dealing with computational burden and different types of data. *Journal of Hydrology*, *281*(4), 251-264.

a mis en forme : Police :12 pt

Meinzer, O. E. (1932). *Outline of methods for estimating ground-water supplies*. Retrieved from

Merritt, M. L. (2004). *Estimating hydraulic properties of the Floridan aquifer system by analysis of earth-tide, ocean-tide, and barometric effects, Collier and Hendry Counties, Florida*: US Department of the Interior, US Geological Survey.

Neuman, S. P. (1972). Theory of flow in unconfined aquifers considering delayed response of the water table. *Water Resources Research, 8*(4), 1031-1045.

Nielsen, P. (1990). Tidal dynamics of the water table in beaches. *Water Resources Research, 26*(9), 2127-2134.

Slooten, L. J., Carrera, J., Castro, E., & Fernandez-Garcia, D. (2010). A sensitivity analysis of tide-induced head fluctuations in coastal aquifers. *Journal of Hydrology, 393*(3-4), 370-380. doi:10.1016/j.jhydrol.2010.08.032.

Solórzano-Rivas, S. C., Werner, A. D., & Irvine, D. J. (2021). Estimating hydraulic properties from tidal propagation in circular islands. Journal of Hydrology, 598, 126182.

Teo, H. T., Jeng, D. S., Seymour, B. R., Barry, D. A., & Li, L. (2003). A new analytical solution for water table fluctuations in coastal aquifers with sloping beaches. *Advances in Water Resources, 26*(12), 1239-1247.

Terzaghi, K. (1954). Anchored bulkheads. *American Society of Civil Engineers Transactions*.

Todd, D. K. (1980). Groundwater Hydrology. *Hydrology, 2nd Edition, John Willey and Sons, 315p*, 235-247.

Vallejos, A., Sola, F., & Pulido-Bosch, A. (2015). Processes influencing groundwater level and the freshwater-saltwater interface in a coastal aquifer. Water Resources Management, 29(3), 679-697.

Van Der Kamp, G. S. (1972). Tidal fluctuations in a confined aquifer extending under the sea. *PROC. LNT. GEOL. CONGR., 24TH SECTION 11 HYDROGEOL*, 101-106.

Van der Kamp, G. S., & Gale, J. E. (1983). Theory of earth tide and barometric effects in porous formations with compressible grains. *Water Resources Research, 19*(2), 538-544.

Werner, A. D., Bakker, M., Post, V. E. A., Vandenbohede, A., Lu, C., Ataie-Ashtiani, B., Simons, C.T., Barry, D. A. (2013). Seawater intrusion processes, investigation and management: Recent advances and future challenges. *Advances in Water Resources, 51*, 3-26. doi:10.1016/j.advwatres.2012.03.004

Zhou, P., Li, G., & Lu, Y. (2016). Numerical modeling of tidal effects on groundwater dynamics in a multi-layered estuary aquifer system using equivalent tidal loading boundary condition: case study in Zhanjiang, China. *Environmental Earth Sciences, 75*(2). doi:10.1007/s12665-015-5034-y

Supplementary materials

To ensure the numerical model accuracy we applied the same boundary conditions as Guarracino et al. (2012) and compared the results. A comparison of amplitudes and time-shift are presented in the figure below.

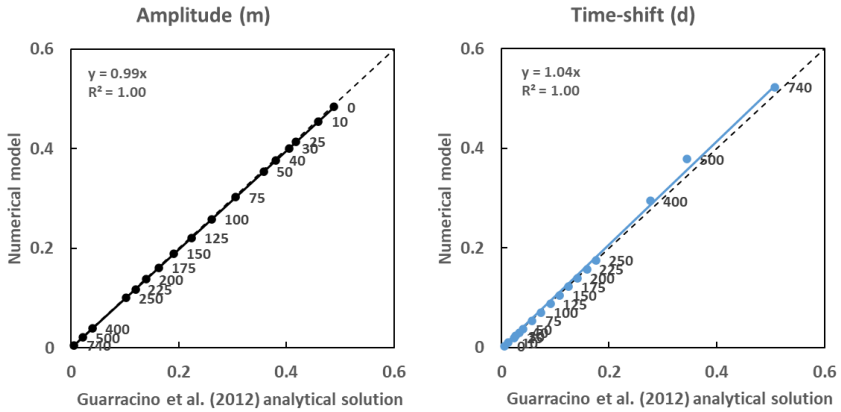

Figure A1: Amplitude and time-shift comparison between our numerical model and the analytical solution of Guarracino et al. (2012). Labels indicates distance from the coastline.

We observed that both the amplitude and the time-shift are well reproduced from the numerical model. Some small differences appear at distance with the time-shift that we attribute to the mesh which has thicker elements from 400 m distance from the coast. However, note that L_c is equal to 250 m.

a mis en forme : Retrait : Première ligne : 1,25 cm